BIOCHEMISTRY
including biophysical chemistry & molecular biology
Article

Biochemistry **2009,** *48,* 9921–9931 9921
DOI: 10.1021/bi901358j

Synergistic Regulation and Ligand-Induced Conformational Changes of Tryptophan Synthase†

M. Qaiser Fatmi, Rizi Ai, and Chia-en A. Chang*

Department of Chemistry, University of California, Riverside, California 92521

Received August 5, 2009; Revised Manuscript Received September 17, 2009

ABSTRACT: Conformational changes of enzyme complexes are often related to regulating and creating an optimal environment for efficient chemistry. We investigated the synergistic regulation of the tryptophan synthase (TRPS) complex, studied for decades as a model of allosteric regulation and substrate channeling within protein complexes. TRPS is a bifunctional tetrameric αββα enzyme complex that exhibits cooperative motions of the α- and β-subunits by tightly controlled allosteric interactions. We have delineated the atomically detailed dynamics and conformational changes of TRPS in the absence and presence of substrates using molecular dynamics simulations. The computed energy and entropy associated with the protein motions also offer mechanistic insights into the conformational fluctuations and the ligand binding mechanism. The flexible α-L6 loop samples both open and partially closed conformations in the ligand-free state but shifts to fully closed conformations when its substrates are present. The fully closed conformations are induced by favorable protein−ligand interactions but are partly compensated by configurational entropy loss. Considerable local rearrangements exist during ligand binding processes when the system is searching for energy minima. The motion of the region that closes the β-subunit during catalysis, the COMM domain, couples with the motion of the α-subunit, although the fluctuations are smaller than in the flexible loop regions. Because of multiple conformations of ligand-free TRPS in the open and partially closed states, the α-L6 loop fluctuations have preferential directionality, which may facilitate the fully closed conformations induced by α- and β-substrates binding to both subunits. Such cooperative and directional motion may be a general feature that contributes to catalysis in many enzyme complexes.

Allosteric communication is important in coordinating function and reactions in many proteins and enzyme complexes. The dynamics and conformational changes in protein structures may range from the fluctuation of side chains to rearrangement of the secondary and tertiary structures (*1*, *2*), which are mandatory for allosteric communication, substrate channeling, and synergistic regulation to optimize protein function (*3*−*10*). A good model system that exhibits all these properties is tryptophan synthase (TRPS),[1] a bifunctional, tetrameric enzyme composed of two α- and two β-subunits. The enzyme complex is arranged in a linear architecture as a αββα complex and catalyzes the last two steps in the biosynthesis of L-tryptophan in prokaryotic and lower eukaryotic organisms (*11*). The centers of the active sites of both α- and β-subunits are far from each other and are connected by a 25 Å long hydrophobic tunnel, which allows for direct substrate channeling of the reaction intermediate without it diffusing into the water. A labeled diagram of a fully functional α/β-dimer of the TRPS complex bound with the ligands 3-indole-D-glycerol-3′-phosphate (IGP) and aminoacrylate (A-A) in their corresponding active sites with important loops and domain coded with different colors is depicted in Figure 1a.

The mechanism of αβ-activation and allosteric regulation in TRPS is associated with an open−closed transition of both subunits (see Figure 1b), which involves large-scale α-L6 motion in the α-subunit, communication domain (COMM domain) motion in the β-subunit, and localized motion of residues at the interface of the α- and β-subunits (*12*−*14*) (see the Supporting Information for the details of the molecular mechanism at the α- and β-sites). Only closed conformations can perform proper catalysis (*15*). The binding of an α-site ligand (ASL) triggers several conformational changes within the binding site that restricts the dynamics of α-L6, which is mandatory for efficient catalysis. These conformational changes in the α-binding site allosterically communicate with the β-site and vice versa, mediating the biosynthesis of L-tryptophan. The overall reaction of TRPS is given in the Supporting Information.

Whether the flexible α-L6 loop exists as an ensemble of open and closed conformations or the closed conformations can be induced only by binding an ASL to the α-site is still debatable. The dynamics of the protein and its contribution to synergy and allostery are unknown, in part due to the fact that the dynamics of TRPS cannot be observed by NMR because of the size of the TRPS complex (∼149 kDa for the αββα structure). Moreover, although high-quality X-ray crystallographic structures are

†Supported by the University of California, Riverside, and the Robert T. Poe Faculty Development Grant from CAFA.

*To whom correspondence should be addressed. E-mail: chiaenc@ucr.edu. Telephone: (951) 827-7263. Fax: (951) 827-4713.

[1]Abbreviations: TRPS, tryptophan synthase; αββα, native form of tryptophan synthase from *Salmonella typhimurium*; α, α-subunit; β, β-subunit; Ain, internal aldimine (Schiff base) intermediate; Aex1, external aldimine intermediate formed between the PLP cofactor and L-Ser; A-A, aminoacrylate Schiff base; Q3, quinonoid intermediate that accumulates during the reaction between A-A and indole; Aex2, L-Trp external aldimine intermediate; PLP, pyridoxal phosphate; IGP, 3-indole-D-glycerol-3′-phosphate; ASL, α-site ligand. Structural elements of tryptophan synthase are designated as follows: loop α-L2, residues α53−60; loop α-L6, residues α179−193; COMM domain, residues β102−189; helix β-H6, residues β165−181.

Published on Web 09/18/2009

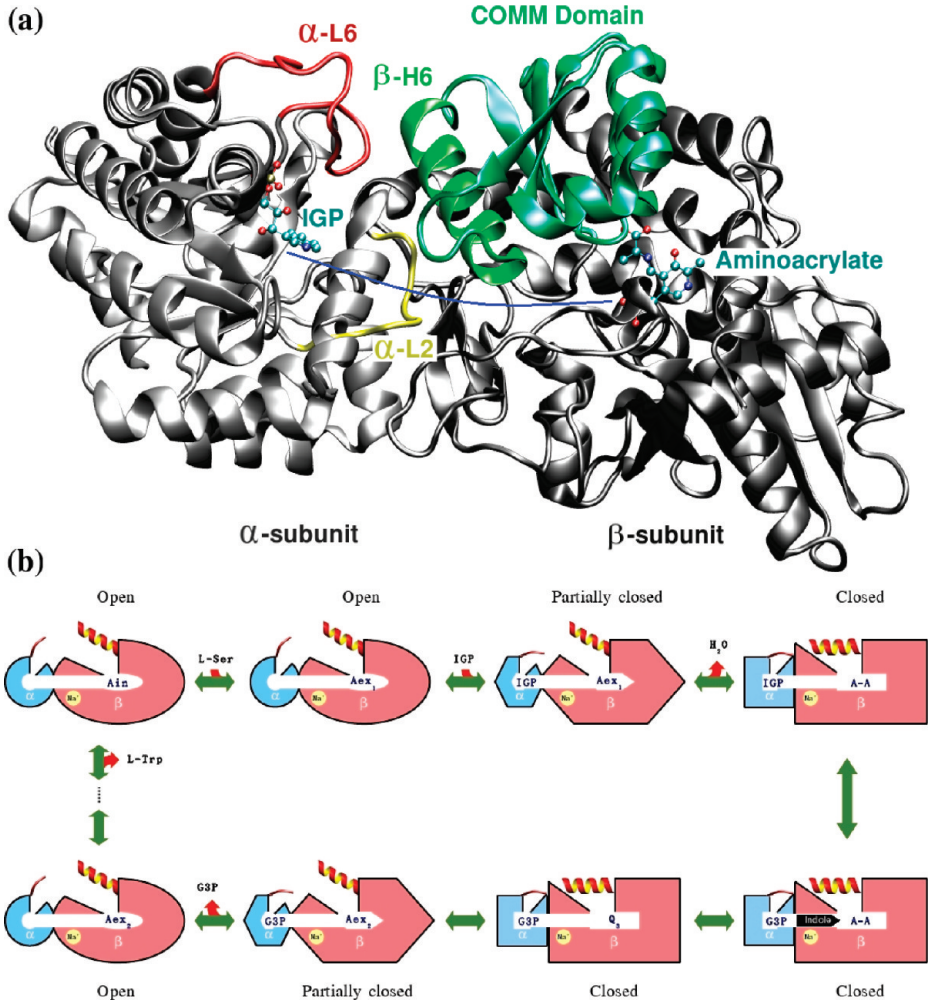

FIGURE 1: (a) Structure of the α/β-dimer of tryptophan synthase with substrates IGP and aminoacrylate shown as a CPK model. The important regions have been coded with different colors: yellow for α-L2 (residues α53−60), red for α-L6 (residues α179−193), green for the COMM domain (residues β102−189), and bright green for β-H6 of the COMM domain (residues β165−181). The approximate location of the interconnecting channel is shown as a solid blue line. These color codes have been used in all graphics. (b) Cartoon representation of synergistic regulation in tryptophan synthase. The α-ligand 3-indole-D-glycerol-3′-phosphate (IGP) splits into glyceraldehyde-3-phosphate (G3P) and indole via the action of the α-subunit. The intermediates internal aldimine (Ain), first external aldimine (Aex_1), and aminoacrylate (A-A) are formed during the stage I β-reaction. The channeling of indole from the α- to β-subunit initiates the stage II β-reaction, which yields L-tryptophan (L-Trp) as a final product through a series of intermediate formations such as Q_3 and Aex_2, for quinonoid and second external aldimine, respectively. Notice the flipping of the α-L6 and β-COMM domain to open and closed conformations and vice versa during the complete biochemical reaction.

available, flexible parts such as open α-L6 (residues 179−192) are missing (see Figure SF1 of the Supporting Information). Therefore, the structure and dynamics of α-L6 in the open state are not recognized, and the processes such as ligand binding and closing of the α-subunit are unknown.

A theoretical study involving the Gaussian network model provided information about the cooperative fluctuations of the α- and β-subunits (*17*). Recently, a molecular dynamics (MD) simulation without a detailed solvent model was used to model the open−closed transition of the α-subunit (*18*). The simulation suggested that the open conformation of α-L6 is favored in wild-type TRPS when ASLs are absent. Several TRPS mutants have been extensively studied (see Table ST1 of the Supporting Information for a brief summary).

To the best of our knowledge, this is the first detailed all-atom explicit water MD simulation study of α/β-dimer of TRPS on the nanosecond scale, where we began to address some fundamental questions underlying allosteric and synergistic regulation. For example, what is the common and special structure and dynamic feature of TRPS? How do α- and β-subunits fluctuate in the ligand-bound and ligand-free states? How do the ligands interact with TRPS, and what conformational changes are observed upon ligand binding? These studies help scientists understand how synergy and allostery are related to the protein function. In this context, we produced three 30−60 ns explicit MD simulations: ligand-free (open state), ligand-bound (partially closed state), and ligand-bound-reference (ligand-bound-ref, completely closed state). We reveal the dynamics and conformational changes induced by ligand binding, particularly the energetic and entropic differences between each state. We also studied the motions of the loops (α-L2 and α-L6) and the COMM domain. Moreover, we compared the distance fluctuations between the key residues, which are responsible for allostery, catalysis, and switching of open and closed states, among simulations.

MATERIALS AND METHODS

Construction of Ligand-Free TRPS with Open α-Subunits and Open β-Subunits. Because crystal structures have only an α-subunit with a closed α-L6 loop, we ran a 15 ns MD simulation with a generalized Born (GB) implicit solvent model

to obtain an open α-L6 loop (*19*). The initial structural coordinates were taken from Protein Data Bank (PDB) entry 2J9X for the α-subunit, and the α-site ligand was manually removed (*20*). The coordinates of three missing residues (Ala190, Leu191, and Pro192) in α-L6 were taken from PDB entry 3CEP (see Figure SF2 of the Supporting Information) (*15*). After a subsequent minimization, equilibration, and MD simulations with the GB model in the Amber package (*21*), several open conformations of the ligand-free α-subunit were collected on the basis of the distance of α-Thr183 (α-L6) and α-Asp60 (α-L2). The open conformations of the ligand-free α-subunit were merged with a ligand-free open β-subunit (PDB entry 1QOQ) to construct several ligand-free TRPS forms with open α-subunits and open β-subunits (*22*). The modeled α/β-dimers underwent energy minimization and equilibration with explicit waters. The systems were then subjected to a minimum of 13−18 ns of explicit MD simulations, and important distances were subsequently analyzed. The most stable α/β-dimer in terms of distance fluctuations was then selected for a 60 ns MD simulation by use of NAMD 2.6 (*23*). Figure SF3 of the Supporting Information shows the steps involved in the MD simulations of the TRPS complex.

Construction of Ligand-Bound TRPS Complexes: Test and Reference Systems. A ligand-bound complex was constructed by placing both α- and β-site ligands in the binding sites. IGP was docked into the α-site of the ligand-free complex obtained from the procedure described in the previous section (the detail parameters of protein−ligand docking are given in the Supporting Information). Since the side chains of the α-site produce considerable changes during the free complex simulation (in particular, α-Phe212), molecular docking programs could not reproduce the crystal structure conformation of IGP. Therefore, the substrate was manually placed into the binding site, and the distance from catalytically important residues α-Asp60 and α-Glu49 to IGP was maintained, as suggested by experiments. The β-site ligand aminoacrylate was docked into the β-subunit of the ligand-free α/β-complex by use of the Autodock4 package (*24*). The choice of IGP and aminoacrylate as ligands for α- and β-sites, respectively, ensures the closed conformation of the α/β-complex. The system containing α- and β-site ligands is termed the ligand-bound complex. After subsequent minimization and equilibration, a 60 ns MD trajectory was collected to observe the possible ligand-induced conformational changes in the complex. Another TRPS system, with IGP and aminoacrylate in the α- and β-sites, respectively, was prepared by using the initial coordinates from a crystal structure (PDB entry 3CEP). This is our reference structure with completely closed α- and β-subunits, which we termed the ligand-bound-ref complex. We created a 30 ns MD simulation after subsequent minimization and equilibration processes.

Molecular Dynamics Simulation Protocol. The ff03 amber force field and general amber force field (GAFF) were applied to all three systems (ligand-free, ligand-bound, and ligand-bound-ref TRPS complexes) (*25*, *26*). The antechamber package was used to create the topology and coordinate files for the ligands (*27*). The protonation states for histidines, aspartates, and glutamates were determined by using MCCE (*28*) and also manually checked by the authors (see Figure SF4 of the Supporting Information). The TRPS complexes contain one α-subunit and one β-subunit. Although no substrates bound to the ligand-free TRPS complex, a pyridoxal 5′-phosphate (PLP) molecule was kept as a cofactor in the β-active site. The system was electronically neutralized by the addition of 14 Na^+ ions. The ligand-bound TRPS complex includes IGP in the α-site and aminoacrylate in the β-site, and the system was neutralized by the addition of 13 Na^+ ions. Both ligand-free and ligand-bound complexes have one Na^+ ion placed close to the β-active site, as suggested in experiments. The ligand-bound-ref complex refers to a completely closed state of TRPS comprised of IGP and aminoacrylate in the α- and β-sites of the complex, respectively. The Cs^+ ion located close to the β-active site in the crystal structure was replaced with the Na^+ ion, and 12 more Na^+ ions were added to neutralize the system. The protonation states of aminoacrylate were calculated by the Mueller group using solid state NMR (see the Supporting Information for details). All the complexes were solvated by a 12 Å TIP3P water box with the xleap program in the amber10 package, and each system has about 86000 atoms.

The initial energy minimization for water molecules was carried out by the sander program (amber10). NAMD version 2.6 was then used for further minimization, equilibration, and production runs. Before equilibration, the systems were gradually heated from 250 to 300 K for 30 ps. The resulting trajectories were collected every 1 ps. The NPT ensemble was applied, and periodic boundary conditions were used throughout the MD simulations. A temperature of 298 K was maintained with a Langevin thermostat with a damping constant of 2 ps^{-1}, and the hybrid Nose-Hoover Langevin piston method was used to control the pressure at 1 atm. The SHAKE algorithm was used to constrain the length of all bonds involving hydrogens; therefore, the time step was set to 2 fs. The nonbonded interactions were truncated at a distance of 14 Å with a switching beginning at 12 Å. The particle mesh Ewald method was used to treat long-range electrostatic interactions beyond the cutoff limit. VMD (*29*) was used for visualization and graphical representation, and the Bio3D package (*30*) was used to analyze simulation results.

Interaction Energy and Entropy Calculation. The total energy $E_{tot}(r)$ can be decomposed into the sum of the potential energy, $U(r)$, and the solvation energy, $W(r)$, both as functions of the coordinate r. The solvation energy comprises a Poisson−Boltzmann term, W_{PB}, for electrostatic solvation free energy (*31*) and a cavity/surface area term, W_{np}, for nonpolar solvation free energy (*32*, *33*). The energy was computed by use of the amber10 package for each snapshot saved during the MD simulations, with waters removed (*21*). The change in mean energy on molecular interactions can be decomposed as follows:

$$\Delta\langle E_{tot}\rangle = \Delta\langle U_c\rangle + \Delta\langle U_{vdw}\rangle + \Delta\langle U_{ele}\rangle + \Delta\langle W_{PB}\rangle + \Delta\langle W_{np}\rangle \quad (1)$$

representing the changes in valence energy (bond, angle, dihedral, and improper dihedral energies), van der Waals (vdw) interactions, Coulombic interactions, and polar solvation and nonpolar solvation free energy, respectively. Each individual interaction energy term is calculated according to the following expressions:

$$\Delta\langle E_{\alpha/\beta\text{-interface}}\rangle = \langle E_{\alpha/\beta\text{-complex}}\rangle - \langle E_{\alpha\text{-subunit}}\rangle - \langle E_{\beta\text{-subunit}}\rangle \quad (2)$$

$$\Delta\langle E_{\text{protein-ligand}}\rangle = \langle E_{\text{subunit with ligand}}\rangle - \langle E_{\text{subunit without ligand}}\rangle - \langle E_{\text{ligand}}\rangle \quad (3)$$

where $\Delta\langle E_{\alpha/\beta\text{-interface}}\rangle$ denotes the interaction energies between the α- and β-subunits and $\Delta\langle E_{\text{protein-ligand}}\rangle$ denotes the energy contributions for a ligand binding to the α- or β-subunit. Note that the valence energy term is canceled during the calculations.

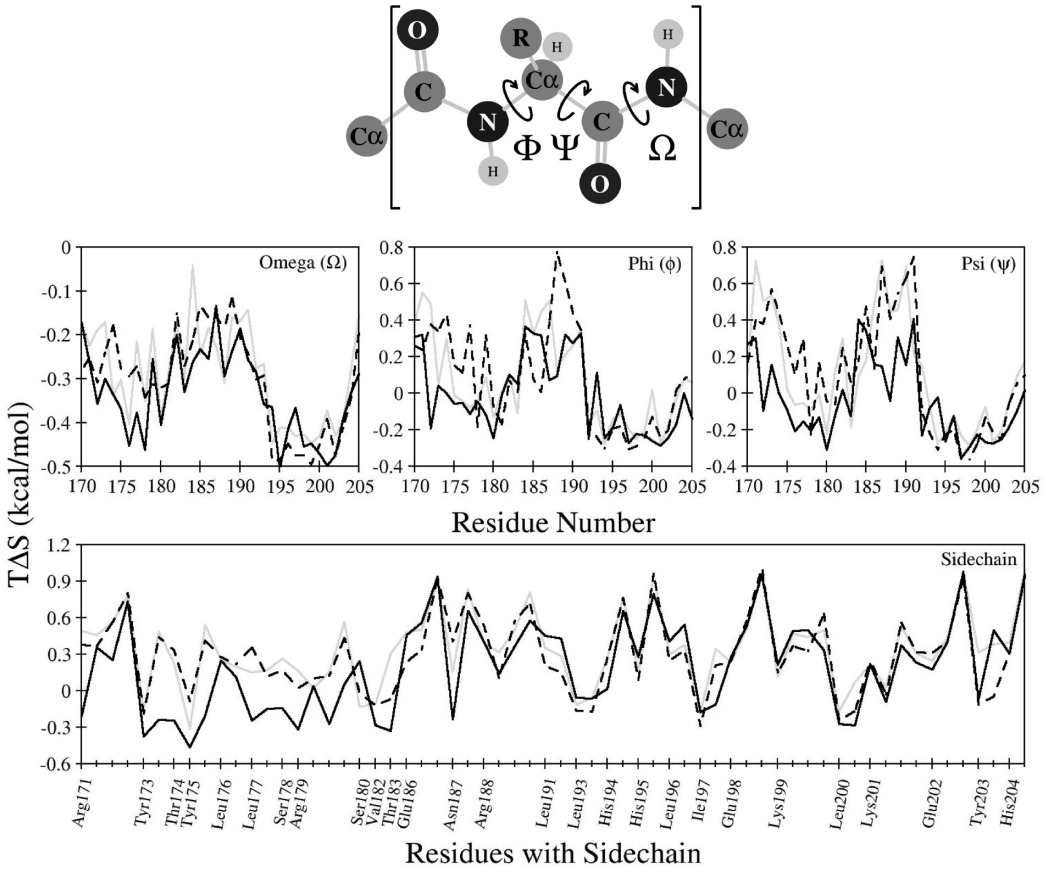

FIGURE 2: Comparison of entropy changes for Ω, Φ, Ψ, and side chain dihedrals associated with α-L6 in ligand-free (gray solid line), ligand-bound (dashed line), and ligand-bound-ref (black solid line) complexes. These definitions apply also to the top panel.

The configurational entropy S includes a conformational part that describes the number of occupied energy wells and a vibrational part that defines the width of each occupied well (*34*−*36*) computed from each dihedral angle. The configurational entropy is calculated by use of the Gibbs entropy formula (*37*):

$$S = -R \int p(x) \ln p(x) \, dx$$

where $p(x)$ is the probability distribution of dihedral x and R is the gas constant. T-analyst was used to compute the Gibbs entropy, and only the internal dihedral degree of freedom of rotatable dihedrals is considered in the entropy calculations. The absolute temperature T is set to 298 K in this study. The change in the configurational entropy of dihedrals of interest between a bound and a free state can be obtained by

$$T\Delta S_{\text{config}} = TS_{\text{bound}} - TS_{\text{free}}$$

RESULTS AND DISCUSSION

In the α-subunit, we denote open, partially closed, and closed α-L6 loops based on two distances (α-L6−β-H6 of the COMM domain and α-L6−α-L2), which are defined by the α-Gly181-(N)−(O)β-Ser178 and α-Asp60(CG)−(OG1)α-Thr183 distances, respectively. We assume that the α-L6 loop is partially closed if the α-L6−β-H6 and α-L6−α-L2 distances are in the range of 3.5−4.2 and 4.0−5.0 Å, respectively. If these distances are shorter than the given range, the α-L6 loops are said to be in closed conformations; otherwise, they are open. In the β-subunit, the definitions of open, partially closed, and closed conformations of the COMM domain are based on the distances of two salt-bridge forming residues, β-Arg141(CZ) and β-Asp305(CG). If the distance is shorter than 5.5 Å or larger than 8.5 Å, the COMM domain is in the closed or open conformation, respectively; otherwise, it is partially closed. On the basis of this definition, only PDB entries 2J9X and 3CEP have closed β-subunit conformations out of 30 wild-type structures, while PDB entry 1QOQ has an open COMM domain conformation in the β-subunit of TRPS. These distance cutoffs have been set after a careful analysis of 50 wild-type and mutated TRPS forms available in the Protein Data Bank.

Dynamics of α-L6. In this study, we were interested in the dynamics of α-L6 (residues 179−193) in TRPS, which plays a crucial role in the regulation of protein function (*11*, *12*). Analysis of the root-mean-square deviation for α-L6, at equilibrium, revealed that the ligand-free TRPS prefers open conformations, but partially closed ("partially open") conformations also exist. However, during a 60 ns ligand-free MD simulation, we could not observe fully closed conformations of α-L6 in TRPS. The fully closed α-L6 may still exist without ASL binding; however, presumably due to high energy barriers, it may not be observed during nanosecond time scale MD stimulations. In our ligand-bound simulation, α-L6 shifted the population toward the closed form but did not completely achieve the fully closed conformation. Our study suggests that instead of being pure random motions, α-L6 fluctuations may have directionality that lets the loop close when substrates bind, which is analogous to population shift or conformational selection models (*4*, *38*−*43*). Still, the fully closed conformations need to be induced by protein−ligand interactions. Similar motions can be found in the COMM domain. Moreover, both α- and β-site ligands allosterically

Table 1: Comparison of Atomic Distance Fluctuations (angstroms) of Key Residues during Ligand-Free, Ligand-Bound, and Ligand-Bound-Ref MD Simulations with Those Obtained from the X-ray Crystallographic Structures of 49 TRPS Conformations[a]

	ligand-free	ligand-bound	ligand-bound-ref	experimental value from PDB crystal structures
α-Gly181(N)−(O)β-Ser178	4.28 ± 0.51	4.03 ± 0.36	3.16 ± 0.31	2.73−3.95[f]
α-Asp60(CG)−(OG1)α-Thr183	5.96 ± 1.48[a]	4.40 ± 1.01[d]	3.79 ± 0.34	3.45−3.91[g]
α-Asp56(CG)−(NZ)β-Lys167	4.45 ± 0.86[b]	4.25 ± 1.13[e]	3.57 ± 0.23	3.02−4.82
β-Arg141(CZ)−(CG)β-Asp305	8.83 ± 2.29[c]	10.17 ± 1.43	5.00 ± 0.54	4.62−13.04

[a]a−e denote average values of two peaks at approximately 3.4 and 6.5 Å, 3.8 and 5.5 Å, 6.6 and 10.5 Å, 3.5 and 5.5 Å, and 3.7 and 5.9 Å, respectively. f and g denote values taken from partially closed and fully closed α-L6 loop conformations of TRPS crystal structures. Open conformations are missing these residues; therefore, these distances are not measurable.

communicate with the other site via changes between the interface. We suggest that the fully closed conformations need to be induced by cooperative motions, and the popular induced-fit model can also be observed in the final stage of the binding processes (*44*). The snapshots for α-L6 dynamics with respect to β-H6 of the COMM domain and α-L2 are shown in Figure SF5 of the Supporting Information.

In Figure 2, computed configurational entropy based on the dihedral degree of freedom is plotted as a function of α-L6 residues; details are given in Table ST2 of the Supporting Information. As expected (*45*), compared to the Φ and Ψ backbone torsional angles, the omega (Ω) dihedral makes the smallest contribution to the α-L6 loop flexibility. The entropy computed for the α-L6 region (residues 170−205 of the α-subunit) decreases by 13 kcal/mol, in comparing the ligand-free TRPS with the ligand-bound-ref state. The value is reduced only slightly, by ∼1 kcal/mol, in a comparison of the ligand-free with the ligand-bound complex. The entropy calculation is based on the sum of the entropy computed from each dihedral angle, and the coupling among dihedrals is neglected here. Therefore, the entropy may be reduced further if dihedral coupling is very strong. Although we anticipated that ligand binding to the α-site would suppress protein motions, thus largely decreasing the entropy of the loop, the ligand-bound complex retains flexibility similar to that in the ligand-free complex. Nevertheless, the ligand-bound-ref complex has very restricted dynamics with small entropy contributions, particularly α-Gly181 and α-Thr183, which form H-bonds with helix β-H6 of the COMM domain. We conclude that our ligand-bound complex is involved in α-ligand binding; therefore, many local rearrangements occur during the simulation, which yields substantial local fluctuations.

Atomic Distance Fluctuations between Key Residues. To demonstrate the protein dynamics, we chose a few key residues reported by experimentalists to illustrate relative protein motions. Mutational studies revealed that residues α-Gly181, β-Ser178, α-Asp60, α-Thr183, α-Asp56, β-Lys167, β-Arg141, and β-Asp305 have vital roles in α-L6 and COMM domain closure and participate in allosteric and synergistic regulations of TRPS. Therefore, the study focused on the dynamics of these residues. Table 1 lists the average atomic distances for key residues involved directly or indirectly in H-bonding obtained from the MD simulations and reported crystal structures, and Figure 3 displays the formation of the H-bond between these residues.

The interaction between α-Gly181(α-L6) and β-Ser178(helix β-H6 of the COMM domain) is responsible for the opening and closing of α-L6 and is involved in the allosteric communication with helix β-H6 of the COMM domain. Figure 4a(i) displays the distance fluctuations for this interaction during the simulation, obtained from ligand-free, ligand-bound, and ligand-bound-ref

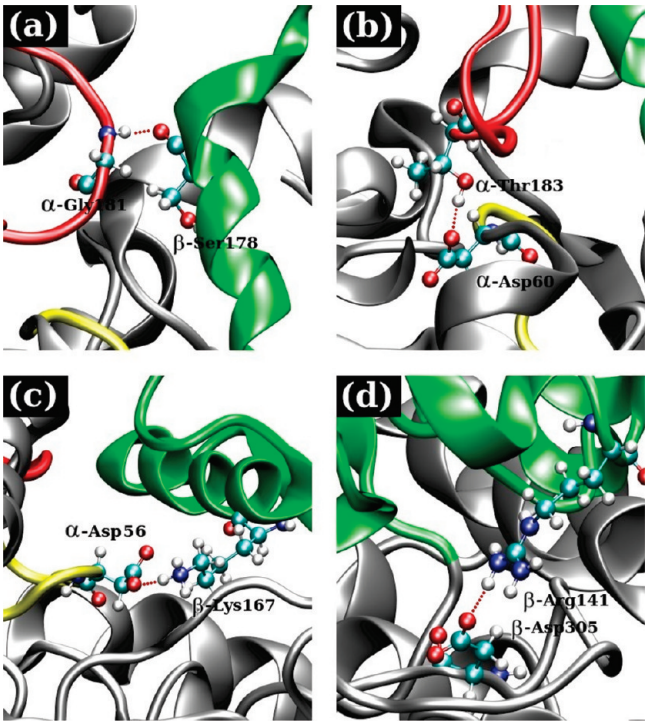

FIGURE 3: Formation of important H-bonds between α-Gly181 and β-Ser178 (a), α-Asp60 and α-Thr183 (b), α-Asp56 and β-Lys167 (c), and β-Arg141 and β-Asp305 (d) to regulate allostery and to control the motion of loops and the COMM domain in TRPS.

MD simulations. The average distance obtained from the ligand-free MD simulation in aqueous solution is 4.28 ± 0.51 Å. This distance cannot be measured experimentally because of missing α-L6 residues in X-ray data, presumably because of their fast motions in the open state. However, as soon as the ligand enters the α-site, this distance begins to decrease (as indicated by the ligand-bound MD simulation, 4.03 ± 0.36 Å) and eventually moves to a completely closed state with the lowest fluctuation, as observed for the ligand-bound-ref simulation (3.16 ± 0.31 Å). This conformational rigidity is a necessary prerequisite for α-catalysis. Analysis of 22 TRPS crystal structures with partially closed or completely closed α-L6 shows this distance ranging from 2.73 to 3.95 Å. Population distribution analysis [Figure 4a(ii)] further clarifies the switching of open α-L6 into closed states upon binding of the α-ligand by shifting the whole population of conformations toward the shorter distances.

Another important interaction responsible for the open and closed α-L6 conformations in TRPS is the intrasubunit α-Asp60(α-L6)−α-Thr183(α-L2) distance. Fluctuations over the simulation time obtained from the three complexes are shown in Figure 4b(i). Because of missing α-L6 residues in the

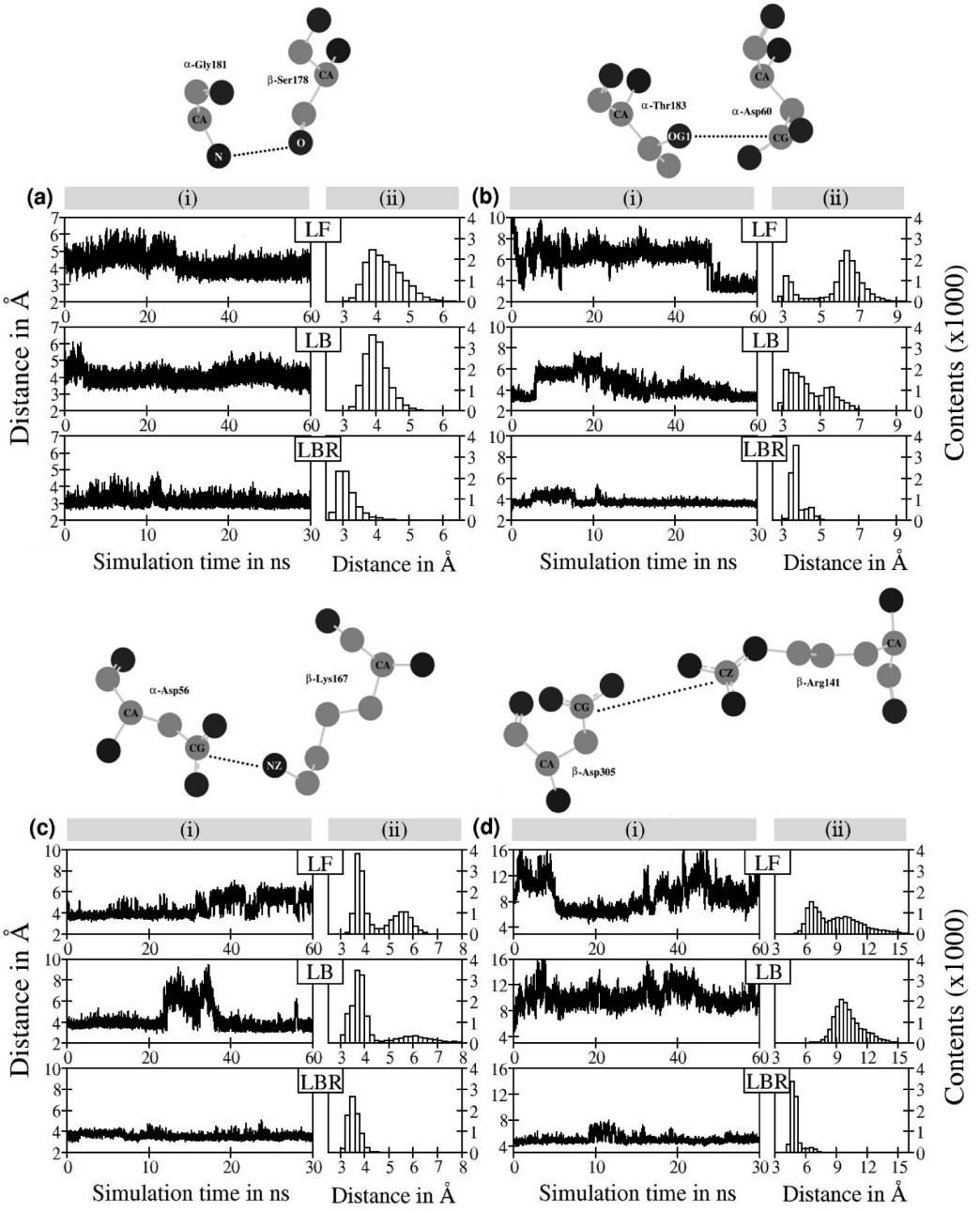

FIGURE 4: Distance plots (i) and corresponding population distributions (ii) for interactions between residues α-Gly181 and β-Ser178 (a), α-Asp60 and α-Thr183 (b), α-Asp56 and β-Lys167 (c), and β-Arg141 and β-Asp305 (d) obtained from ligand-free (LF), ligand-bound (LB), and ligand-bound-ref (LBR) MD simulations.

experimental data for open conformations, no information about this distance is available for open α-L6. However, for partially closed or completely closed α-L6, the reported distance ranges from 3.45 to 3.91 Å. The 60 ns MD simulation of the ligand-free complex yields an average distance of 5.96 ± 1.48 Å, which is substantially longer than those reported for partially closed and completely closed conformations (3.45−3.91 Å), which indicates the dominance of the open α-L6 conformation in the ligand-free state. In the ligand-bound state, this distance gradually decreases to a smaller value (4.40 ± 1.01 Å) and further reduces to 3.79 ± 0.34 Å for ligand-bound-ref complexes. The population distributions [Figure 4b(ii)] further verify the switching of α-L6 from an open to a closed conformation upon ligand binding. The narrower distributions in the ligand-bound-ref complex explain the rigidity of α-L6 in the presence of α-ligand.

In addition to several local conformational changes, the binding of ASLs also induces many global effects. Figure 4c(i) shows the fluctuations in the α-Asp56−β-Lys167 distance, which represent intersubunit motions. The corresponding population distributions are given in Figure 4c(ii). The interaction between α-Asp56(L2) and β-Lys167(helix β-H6 of the COMM domain) is important for allosteric communication, and mutations of either residue weaken the ability of the α-subunit to activate the β-subunit (or to close the β-subunit), thus altering the reaction rate of the β-subunit. Analysis of 45 crystal structures of TRPS shows a range of this distance of 3.02−4.82 Å. The MD simulations of ligand-free, ligand-bound, and ligand-bound-ref complexes yield this distance as an average of 4.45 ± 0.86 Å (an average over two peaks at distances of ~3.8 and ~5.5 Å), 4.25 ± 1.13 Å (an average of two peaks at ~3.7 and ~5.9 Å), and 3.57 ± 0.23 Å, respectively. Considering the average values of this

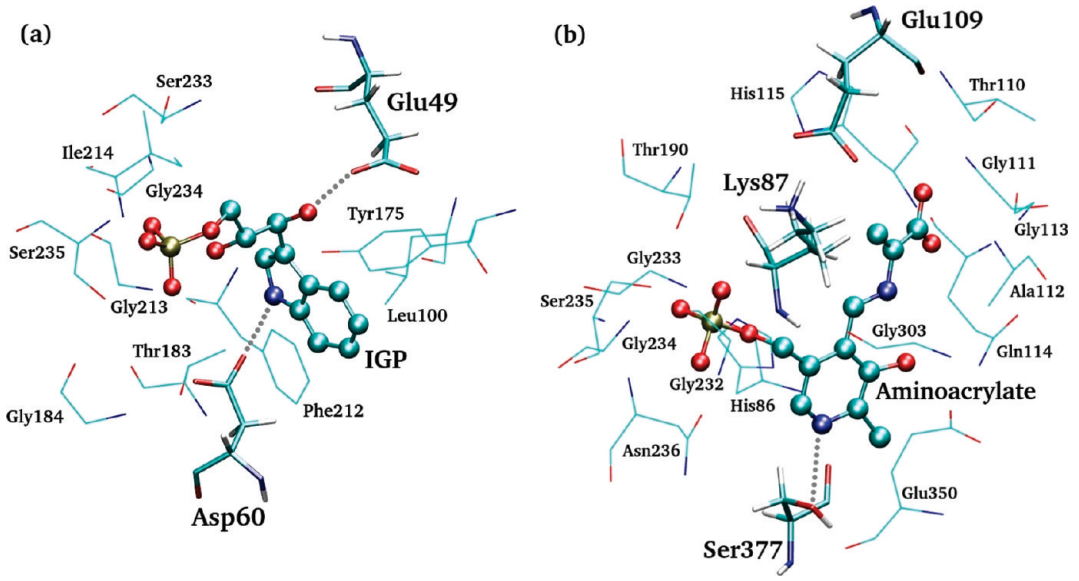

FIGURE 5: Snapshots of (a) α- and (b) β-active sites in the presence of 3-indole-D-glycerol-3′-phosphate (IGP) and aminoacrylate as α- and β-site ligands (shown in CPK), respectively. Residues involved directly in the catalysis are shown as licorice. The gray dotted lines indicate the stable interactions between residual atoms and ligand atoms [i.e., α-Asp60(OD1)−(NE1)IGP and α-Glu49(OE1)−(O3)IGP in the α-subunit and β-Ser377(OG)−(N1)aminoacrylate in the β-subunit].

distance, apparently binding of ASLs strengthens the α-Asp56−β-Lys167 interaction, as reflected by the shorter distances in the ligand-bound and ligand-bound-ref complexes as compared to that in the ligand-free complex. The population distributions for the α-Asp56−β-Lys167 distance depicted in Figure 4c(ii) further verify it by shifting the larger distance into the smaller distance upon ligand binding. However, for the ligand-bound complex, larger intersubunit fluctuations can be observed, which indicates the system is in search of more stable conformations.

Unlike α-L6, the COMM domain is mainly composed of α-helices and β-sheets that lead to relatively restricted dynamics of the residues. The open and closed conformations of the β-subunit are, therefore, barely distinguishable. Thus, as suggested by experiments, the distance between β-Arg141 and β-Asp305 is used to define the open and closed conformations of the β-subunit. With this definition, only two (PDB entries 2J9X and 3CEP) of 30 wild-type crystal structures of TRPS have a completely closed β-subunit, and the β-Arg141−β-Asp305 distances are 4.85 and 4.68 Å, respectively. The remaining crystal structures show a longer β-Arg141−β-Asp305 distance, ranging from 6.93 to 13.04 Å. Figure 4d indicates that the β-Arg141−β-Asp305 distance fluctuates and is on average 8.83 ± 2.29 Å (average of two peaks at ~6.6 and ~10.5 Å), 10.17 ± 1.43 Å, and 5.00 ± 0.54 Å for the ligand-free, ligand-bound, and ligand-bound-ref complexes, respectively. Our simulation reveals that the β-Arg141−β-Asp305 distance in the ligand-free TRPS fluctuates between two distinct conformations, fully open and partially closed. However, the ligand-bound-ref complex produces only a single peak at a shorter β-Arg141−β-Asp305 distance (5.00 ± 0.54 Å), which indicates the dominance of the closed β-subunit in the presence of ligands. Notably, the β-subunit of our ligand-bound model stays in a fully open conformation, even when both substrates are present. We surmise that the closure of the COMM domain may require a longer trajectory of a few microseconds to yield fully closed β-subunit conformations.

Ligand−Protein Interactions. The binding of IGP and aminoacrylate to the active sites induces closed conformations to enhance the catalytic rate. In the α-site, α-Glu49 and α-Asp60 are reported as catalytically relevant residues, which contribute directly to the cleavage of IGP into G3P and indole. Other residues help maintain the hydrophilic and hydrophobic interactions with the IGP and, therefore, provide a feasible environment for the biocatalysis. Figure 5a displays the important interactions of IGP with α-site residues, and Figure 6a,b shows distance fluctuations of IGP with α-Glu49 and α-Asp60 obtained from the ligand-bound and ligand-bound-ref simulations. In the ligand-bound simulation, IGP has unexpected distance fluctuations with respect to α-Glu49 and α-Asp60. Such fluctuations are associated with local rearrangements to find suitable interactions. The ligand-bound-ref complex, however, yields a highly conserved and stable distance with very small fluctuations for both α-Glu49−IGP (2.61 ± 0.09 Å) and α-Asp60−IGP (2.96 ± 0.33 Å) distances throughout the 30 ns simulation.

In the β-site, β-Ser377 may form a very stable H-bond with the intermediate to stabilize the electronic charges on transition states (*46*, *47*). Therefore, the distance between the pyridine nitrogen of aminoacrylate (or PLP) and β-Ser377 was studied to determine the dynamics of the ligand and the local residues. In nearly 40 crystal structures, the experimentally observed distance varied from 2.56 to 3.07 Å. The average distance in the ligand-free MD simulation (β-Ser377−PLP) is 3.08 ± 0.45 Å (Figure 6c). The distance slightly increases upon binding of the β-ligand (3.89 ± 0.99 Å) as shown in ligand-bound simulation because of the local rearrangement to find favorable interactions. After the complex achieves one of the global energy minima, such as the ligand-bound-ref complex in this study, the distance decreases to an average of 2.88 ± 0.12 Å. Forming an H-bond, as shown in Figure 5, is necessary to carry out the β-reaction, which also contributes to the conformational stability and results in smaller local fluctuations.

Table 2 lists the energies of ligand−protein interactions. Although ligand−protein binding presumably forms negative interaction energies, this occurs only when the optimal geometries are attained. For example, the interaction energies of the ligand-bound-ref complex are −3 and −35 kcal/mol for α- and

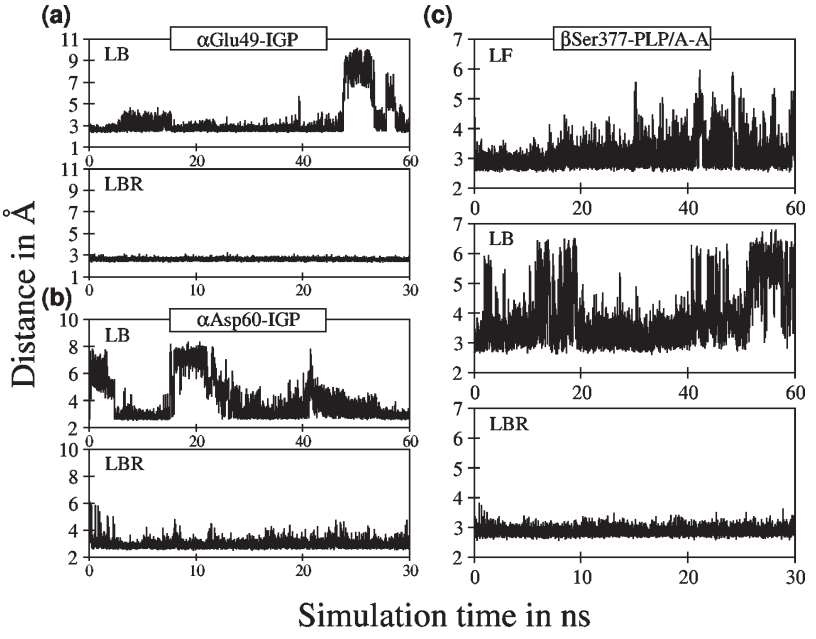

FIGURE 6: Ligand−protein distance plots for α-Glu49(OE1)−(O3)IGP (a), α-Asp60(OD1)−(NE1)IGP (b), and β-Ser377(OG)−(N1)PLP/A-A (c) interactions obtained from ligand-free (LF), ligand-bound (LB), and ligand-bound-ref (LBR) MD simulations. IGP, PLP, and A-A denote 3-indole-D-glycerol-3′-phosphate, pyridoxal 5′-phosphate, and aminoacrylate, respectively.

β-ligands, respectively. The favorable interactions also ensure the next step of the catalytic cycle. In contrast, during the ligand binding processes, the searching of local energy minima for the complex incurs large-scale conformational changes, as described previously. Although when aminoacrylate was docked into the β-subunit, the interaction energies were negative, aminoacrylate still does not form perfect contacts with the protein, due to the protein side chain rearrangement during the ligand-free MD simulation. Therefore, both aminoacrylate and protein fluctuate significantly during the binding process. This stage may also produce less favorable ligand−protein interaction energies, primarily by losing H-bonds between ligands and the protein's active sites (6.3 and 25.8 kcal/mol for α- and β-ligands, respectively). The unfavorable interactions are compensated in part by an increase in local entropy and by induction of stronger intersubunit interaction in the α-site−β-site interface, as we discuss in the next section.

Interaction Energy Contribution at the α−β-Interface. Changes of interaction energies in the α-site−β-site interface are directly related to the communication between the α- and β-subunits. As expected, van der Waals interactions play a key role in the α-subunit−β-subunit association in all three complexes, because the dimer dominantly has hydrophobic residues in the interface. The interaction becomes stronger from the ligand-free (−141.7 kcal/mol) to ligand-bound (−156.1 kcal/mol) and ligand-bound-ref (−162.9 kcal/mol) complexes. A similar trend can be found in Coulombic interactions (see Table 2 for details). The Coulombic U_{ele} and electrostatic solvation terms (W_{PB}) appear to be remarkably well balanced (*48*); therefore, we considered the sum of both terms here ($\Delta\langle U_{ele} + W_{PB}\rangle$) to study the electrostatic contributions. Interestingly, $\Delta\langle U_{ele} + W_{PB}\rangle$ contributes approximately −85 kcal/mol to attract the α- and β-subunits in both ligand-free and ligand-bound-ref complexes. In the ligand-bound complex, the binding of substrates perturbs the α-site−β-site interface, and the conformational arrangement is associated with particularly strong $\Delta\langle U_{ele} + W_{PB}\rangle$ interactions (approximately −106 kcal/mol). Of note, although the ligand-bound-ref complex does not yield the lowest interaction energies in the α-site−β-site interface, the overall changes in interaction energies are favorable, because of ligand−protein attractions.

Table 2: Interaction Energy Contributions (kilocalories per mole) to α/β-Subunit Association in the TRPS Enzyme and Ligand−Protein Interactions in the α- and β-Active Sites

complex	ligand	ΔU_{vdw}	ΔU_{ele}	ΔW_{PB}	ΔW_{np}	ΔE_{tot}
			α/β-Interface			
ligand-free	−	−141.7	101.4	−186.6	102.3	−124.6
ligand-bound	−	−156.1	−20.1	−84.3	109.8	−150.7
ligand-bound-ref	−	−162.9	−97.5	12.2	108.3	−139.9
			Protein−Ligand			
ligand-bound	α	−33.6	−66.6	87.7	18.8	6.3
	β	−41.9	−89.8	134.3	23.2	25.8
ligand-bound-ref	α	−42.6	−57.5	77.4	19.7	−3.0
	β	−38.6	−197.4	178.9	21.3	−35.0

The energy calculations suggest that the binding of the substrates generates a certain rearrangement near the interface before the complex finds the global energy minima. Nevertheless, the binding eventually stabilizes the entire complex, which also increases the α-subunit−β-subunit allosteric communication and helps to close the subunits for the catalysis.

Cooperative Fluctuation of α- and β-Subunits: Principal Component and Dynamical Cross-Correlation Matrix Analysis. To identify the most common patterns of α/β-motions in the TRPS complex, principal component analysis (PCA) was conducted on trajectories obtained from the MD simulations. PCA is a useful statistical technique that reduces a complex and high-dimension data set to a simple and lower-dimension data set that reveals dominant patterns. Figure 7a shows a snapshot of the PCA calculation of the ligand-free complex. PCA of the ligand-bound and ligand-bound-ref complexes revealed similar dominant modes of motion but with

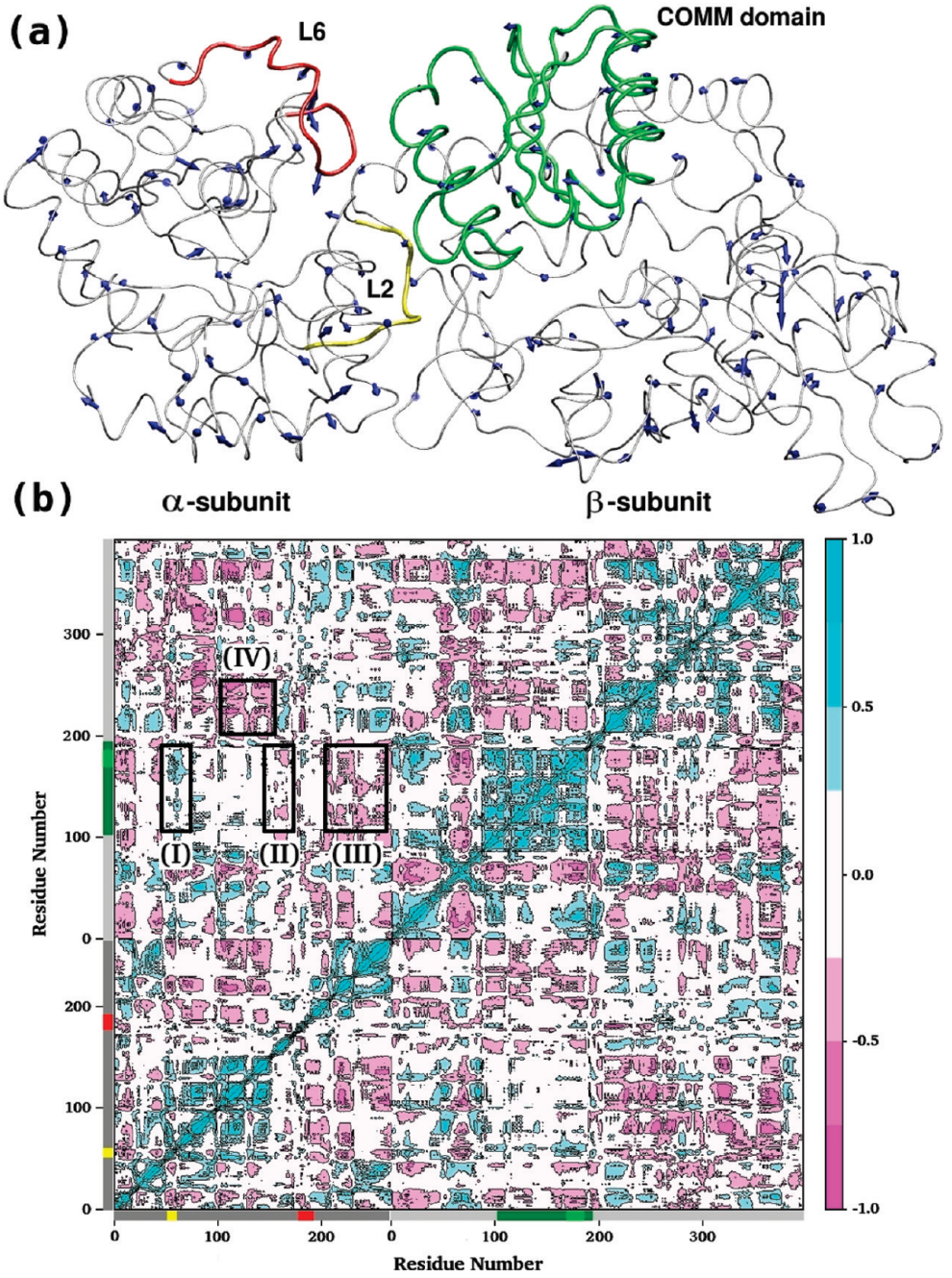

FIGURE 7: (a) Dominant mode of motions of α-L6, α-L2, and the COMM domain from principal component analysis. (b) Residue−residue plot of the cross-correlation matrix. Both plots are generated from the ligand-free TRPS MD simulation. The color scale in panel b runs from pink (−1 to −0.75) to white (−0.25 to 0.25) to cyan (0.75−1). Negative values (pink) indicate that Cα atoms move along opposite directions, namely anticorrelated motions, whereas positive values (cyan) represent correlated motions occurring along the same direction. Important correlated−anticorrelated motions across the subunits are labeled from I to IV. Yellow, red, green, and bright green are the color codes for α-L2, α-L6, the COMM domain, and *β*-H6 of the COMM domain, respectively.

smaller magnitudes (data not shown) because of the partially closed or fully closed conformations upon binding of ligands, which restrict the motion of loops and the COMM domain. Figure 7a demonstrates the strong tendency of loops α-L6 and α-L2 and the COMM domain to move in concert (blue arrows). This synergistic movement of α-L6 and α-L2 squeezes the α-ligand and facilitates the formation of the fully closed conformation to catalyze the α-reaction. The inclination of the COMM domain in the direction of the α-subunit may mediate protein allosteric communication and, again, induce the fully closed conformation and thereby enhance the overall rate of the α/*β*-reaction.

The correlation of the displacements of all residue pairs depicted in Figure 7b clearly indicates a strong correlation between α-L2 and the COMM domain (labeled I). Moreover, the α-L6 loop exhibits only a weak correlated motion with the COMM domain, possibly because of its highly flexible nature. However, the residues at both edges of α-L6 display strong negative cross-correlations (labeled as II and III) with the COMM domain and are consistent with the PCA results. Apart from the loops and the COMM domain, the other parts of the α-subunit also exhibit correlated motions with the *β*-subunit (see label IV, for example). Such correlated motions of the whole subunits are directly related to synergism.

CONCLUSIONS

In this work, we have studied the structure and dynamics of key residues for the α/β-dimer of TRPS and, consequently, the motion of α-L6 and the COMM domain in ligand-free, ligand-bound, and ligand-bound-ref complexes. Notably, the dynamic features illustrated by our simulations are challenging to obtain experimentally, even with recent advanced experimental techniques. The comparative studies for all three complexes clearly show that switching between the open and closed conformations of α-L6 is associated with substrate binding, which is largely due to the perturbed backbone motions and side chain reorganization. In the ligand-free state, both α- and β-subunits exist in various conformations, including open and partially closed, with the open states being the most dominant. However, no fully closed conformations were observed during the ligand-free MD simulation. In the ligand-bound-ref complex, the ligand−protein interactions induce fully closed conformations. The fully closed conformations encapsulate substrates and intermediates from escaping into the solvent and provide an environment for catalysis. Our ligand-bound simulation revealed possible substrate binding processes that undergo considerable local reorganization.

The ligands binding to both α- and β-subunits not only constrain the flexibility of residues in active sites but also bring both subunits closer as well, suggesting significant allosteric communication in this system. These global effects are reflected by shorter distances between key residues (Gly181−Ser178 and Asp56−Lys167) and more negative interaction energies in the α/β-dimer interface in the ligand-bound-ref complexes, compared with the ligand-free protein.

Further analysis of TRPS conformational changes suggests a different scenario for the substrate binding mechanisms, which combines both population shift and induced-fit models. Moreover, we observed cooperative motions between the subunits, and such synergistic regulation is a prerequisite for efficient catalysis and substrate channeling processes.

ACKNOWLEDGMENT

We thank Drs. Michael F. Dunn and Dimitri Niks for valuable suggestions and discussion, Leonard Mueller and Jinfeng Lai for discussion and for providing the protonation state of aminoacrylate, and Ray Luo for helping with solvation energy calculations. We also thank the National Center for Supercomputing Application for computational resources.

SUPPORTING INFORMATION AVAILABLE

Additional methods and results. This material is available free of charge via the Internet at http://pubs.acs.org.

REFERENCES

1. James, L. C., and Tawfik, D. S. (2003) Conformational diversity and protein evolution: A 60-year-old hypothesis revisited. *Trends Biochem. Sci. 28*, 361–368.
2. Bhardwaj, N., and Gerstein, M. (2009) Relating protein conformational changes to packing efficiency and disorder. *Protein Sci. 18*, 1230–1240.
3. Tsai, C.-J., del Sol, A., and Nussinov, R. (2008) Allostery: Absence of a Change in Shape Does Not Imply that Allostery Is Not at Play. *J. Mol. Biol. 378*, 1–11.
4. Henzler-Wildman, K. A., Thai, V., Lei, M., Ott, M., Wolf-Watz, M., Fenn, T., Pozharski, E., Wilson, M. A., Petsko, G. A., Karplus, M., Hubner, C. G., and Kern, D. (2007) Intrinsic motions along an enzymatic reaction trajectory. *Nature 450*, 838–843.
5. Cheng, Y. H., Chang, C. E. A., Yu, Z. Y., Zhang, Y. J., Sun, M. H., Leyh, T. S., Holst, M. J., and McCammon, J. A. (2008) Diffusional Channeling in the Sulfate-Activating Complex: Combined Continuum Modeling and Coarse-Grained Brownian Dynamics Studies. *Biophys. J. 95*, 4659–4667.
6. Chen, J., Dima, R. I., and Thirumalai, D. (2007) Allosteric communication in dihydrofolate reductase: Signaling network and pathways for closed to occluded transition and back. *J. Mol. Biol. 374*, 250–266.
7. Hyeon, C., Jennings, P. A., Adams, J. A., and Onuchic, J. N. (2009) Ligand-induced global transitions in the catalytic domain of protein kinase A. *Proc. Natl. Acad. Sci. U.S.A. 106*, 3023–3028.
8. Pontiggia, F., Zen, A., and Micheletti, C. (2008) Small- and Large-Scale Conformational Changes of Adenylate Kinase: A Molecular Dynamics Study of the Subdomain Motion and Mechanics. *Biophys. J. 95*, 5901–5912.
9. Singh, N., and Briggs, J. M. (2008) Molecular Dynamics Simulations of Factor Xa: Insight into Conformational Transition of Its Binding Subsites. *Biopolymers 89*, 1104–1113.
10. Mitra, A., and Sept, D. (2008) Taxol Allosterically Alters the Dynamics of the Tubulin Dimer and Increases the Flexibility of Microtubules. *Biophys. J. 95*, 3252–3258.
11. Barends, T. R. M., Dunn, M. F., and Schlichting, I. (2008) Tryptophan synthase, an allosteric molecular factory. *Curr. Opin. Chem. Biol. 12*, 593–600.
12. Dunn, M. F., Niks, D., Ngo, H., Barends, T. R., and Schlichting, I. (2008) Tryptophan Synthase: The Workings of a Channeling Nanomachine. *Trends Biochem. Sci. 33*, 254–264.
13. Rhee, S., Parris, K. D., Hyde, C. C., Ahmed, S. A., Miles, E. W., and Davies, D. R. (1997) Crystal structures of a mutant (βK87T) tryptophan synthase $\alpha_2\beta_2$ complex with ligands bound to the active sites of the α- and β-subunits reveal ligand-induced conformational changes. *Biochemistry 36*, 7664–7680.
14. Schneider, T. R., Gerhardt, E., Lee, M., Liang, P. H., Anderson, K. S., and Schlichting, I. (1998) Loop closure and intersubunit communication in tryptophan synthase. *Biochemistry 37*, 5394–5406.
15. Barends, T. R. M., Domratcheva, T., Kulik, V., Blumenstein, L., Niks, D., Dunn, M. F., and Schlichting, I. (2008) Structure and mechanistic implications of a tryptophan synthase quinonold intermediate. *ChemBioChem 9*, 1024–1028.
16. Lane, A. N., and Kirschner, K. (1991) Mechanism of the Physiological Reaction Catalyzed by Tryptophan Synthase from *Escherichia coli*. *Biochemistry 30*, 479–484.
17. Bahar, I., and Jernigan, R. L. (1999) Cooperative fluctuations and subunit communication in tryptophan synthase. *Biochemistry 38*, 3478–3490.
18. Spyrakis, F., Raboni, S., Cozzini, P., Bettati, S., and Mozzarelli, A. (2006) Allosteric communication between α and β subunits of tryptophan synthase: Modelling the open-closed transition of the α subunit. *Biochim. Biophys. Acta 1764*, 1102–1109.
19. Onufriev, A., Bashford, D., and Case, D. A. (2000) A Modification of the Generalized Born Model Suitable for Macromolecules. *J. Phys. Chem. B 104*, 3712–3720.
20. Ngo, H., Harris, R., Kimmich, N., Casino, P., Niks, D., Blumenstein, L., Barends, T. R., Kulik, V., Weyand, M., Schlichting, I., and Dunn, M. F. (2007) Synthesis and characterization of allosteric probes of substrate channeling in the tryptophan synthase bienzyme complex. *Biochemistry 46*, 7713–7727.
21. Case, D. A., Cheatham, T. E., Darden, T., Gohlke, H., Luo, R., Merz, K. M., Onufriev, A., Simmerling, C., Wang, B., and Woods, R. J. (2005) The Amber biomolecular simulation programs. *J. Comput. Chem. 26*, 1668–1688.
22. Weyand, M., and Schlichting, I. (1999) Crystal structure of wild-type tryptophan synthase complexed with the natural substrate indole-3-glycerol phosphate. *Biochemistry 38*, 16469–16480.
23. Phillips, J. C., Braun, R., Wang, W., Gumbart, J., Tajkhorshid, E., Villa, E., Chipot, C., Skeel, R. D., Kale, L., and Schulten, K. (2005) Scalable molecular dynamics with NAMD. *J. Comput. Chem. 26*, 1781–1802.
24. Morris, G. M., Huey, R., Lindstrom, W., Sanner, M. F., Belew, R. K., Goodsell, D. S., and Olson, A. J. (2009) AutoDock4 and Auto DockTools4: Automated Docking with Selective Receptor Flexibility. *J. Comput. Chem.* (in press).
25. Wang, J. M., Wolf, R. M., Caldwell, J. W., Kollman, P. A., and Case, D. A. (2004) Development and testing of a general amber force field. *J. Comput. Chem. 25*, 1157–1174.
26. Hornak, V., Abel, R., Okur, A., Strockbine, B., Roitberg, A., and Simmerling, C. (2006) Comparison of multiple amber force fields and development of improved protein backbone parameters. *Proteins: Struct., Funct., Bioinf. 65*, 712–725.

27. Wang, J. M., Wang, W., Kollman, P. A., and Case, D. A. (2006) Automatic atom type and bond type perception in molecular mechanical calculations. *J. Mol. Graphics Modell. 25*, 247–260.
28. Song, Y. F., and Gunner, M. R. (2009) Using Multiconformation Continuum Electrostatics to Compare Chloride Binding Motifs in α-Amylase, Human Serum Albumin, and Omp32. *J. Mol. Biol. 387*, 840–856.
29. Humphrey, W., Dalke, A., and Schulten, K. (1996) VMD: Visual Molecular Dynamics. *J. Mol. Graphics 14*, 33–38.
30. Grant, B. J., Rodrigues, A. P. C., ElSawy, K. M., McCammon, J. A., and Caves, L. S. D. (2006) Bio3d: An R package for the comparative analysis of protein structures. *Bioinformatics 22*, 2695–2696.
31. Luo, R., David, L., and Gilson, M. K. (2002) Accelerated Poisson-Boltzmann calculations for static and dynamic systems. *J. Comput. Chem. 23*, 1244–1253.
32. Sitkoff, D., Sharp, K. A., and Honig, B. (1994) Accurate Calculation of Hydration Free-Energies Using Macroscopic Solvent Models. *J. Phys. Chem. 98*, 1978–1988.
33. Tan, C., Tan, Y. H., and Luo, R. (2007) Implicit nonpolar solvent models. *J. Phys. Chem. B 111*, 12263–12274.
34. Hnizdo, V., Tan, J., Killian, B. J., and Gilson, M. K. (2008) Efficient calculation of configurational entropy from molecular simulations by combining the mutual-information expansion and nearest-neighbor methods. *J. Comput. Chem. 29*, 1605–1614.
35. Chang, C.-E. A., McLaughlin, W. A., Baron, R., Wang, W., and McCammon, J. A. (2008) Entropic contributions and the influence of the hydrophobic environment in promiscuous protein-protein association. *Proc. Natl. Acad. Sci. U.S.A. 105*, 7456–7461.
36. Meirovitch, H. (2007) Recent developments in methodologies for calculating the entropy and free energy of biological systems by computer simulation. *Curr. Opin. Struct. Biol. 17*, 181–186.
37. Dill, K. A., and Bromberg, S. (2003) Molecular Driving Forces , Garland Science, London.
38. Arora, K., and Brooks, C. L. (2007) Large-scale allosteric conformational transitions of adenylate kinase appear to involve a population-shift mechanism. *Proc. Natl. Acad. Sci. U.S.A. 104*, 18496–18501.
39. Ravindranathan, K. P., Gallicchio, E., and Levy, R. M. (2005) Conformational equilibria and free energy profiles for the allosteric transition of the ribose-binding protein. *J. Mol. Biol. 353*, 196–210.
40. Gsponer, J., Christodoulou, J., Cavalli, A., Bui, J. M., Richter, B., Dobson, C. M., and Vendruscolo, M. (2008) A coupled equilibrium shift mechanism in calmodulin-mediated signal transduction. *Structure 16*, 736–746.
41. Okazaki, K. I., and Takada, S. (2008) Dynamic energy landscape view of coupled binding and protein conformational change: Induced-fit versus population-shift mechanisms. *Proc. Natl. Acad. Sci. U.S.A. 105*, 11182–11187.
42. Swift, R. V., and McCammon, J. A. (2009) Substrate Induced Population Shifts and Stochastic Gating in the PBCV-1 mRNA Capping Enzyme. *J. Am. Chem. Soc. 131*, 5126–5133.
43. Wong, S., and Jacobson, M. P. (2008) Conformational selection in silico: Loop latching motions and ligand binding in enzymes. *Proteins 71*, 153–164.
44. Grunberg, R., Leckner, J., and Nilges, M. (2004) Complementarity of structure ensembles in protein-protein binding. *Structure 12*, 2125–2136.
45. Shen, T., Hamelberg, D., and McCammon, J. A. (2006) Elasticity of peptide omega bonds. *Phys. Rev. E 73*, 041908–041913.
46. Hyde, C. C., Ahmed, S. A., Padlan, E. A., Miles, E. W., and Davies, D. R. (1988) Three-Dimensional Structure of the Tryptophan Synthase $\alpha_2\beta_2$ Multienzyme Complex from *Salmonella typhimurium*. *J. Biol. Chem. 263*, 17857–17871.
47. Jhee, K. H., Yang, L. H., Ahmed, S. A., McPhie, P., Rowlett, R., and Miles, E. W. (1998) Mutation of an active site residue of tryptophan synthase (β-serine 377) alters cofactor chemistry. *J. Biol. Chem. 273*, 11417–11422.
48. Chang, C. E., and Gilson, M. K. (2004) Free energy, entropy, and induced fit in host-guest recognition: Calculations with the second-generation mining minima algorithm. *J. Am. Chem. Soc. 126*, 13156–13164.